Pore Structure of Thermally Treated Goethite (α-FeOOH)

JOSE L. RENDON,*[,1] JUAN CORNEJO,* PABLO DE ARAMBARRI,* AND CARLOS J. SERNA†

*Centro de Edafología y Biología Aplicada del Cuarto, C.S.I.C. Apdo. 1052, Sevilla; and †Grupo de Fisicoquímica Mineral, C.S.I.C. Serrano, 115—dpdo, Madrid—6, Spain

Received March 22, 1982; accepted June 18, 1982

The thermal decomposition of synthetic α-FeOOH in air has been studied by X-ray powder diffraction (XRD), IR spectroscopy, transmission electron microscopy, and nitrogen adsorption. Three stages may be differentiated during the course of the reaction: (i) *200–250°C*; slit-shaped micropores of nearly equal width, about 1.4 nm, are formed along the elongated direction of the lath-shaped acicular microcrystals of the hematite products, the highest surface area is obtained on a α-FeOOH decomposed at 250°C; (ii) *300–600°C*; an internal sintering occurs within the microcrystals transforming the micropores into closed spherical mesopores with the consequent significant decrease in surface area; and (iii) *above 600°C*; interparticle sintering takes place and no valuable porosity is detected. Particle shape effects are shown to be the reason for the differences in the IR spectra and for the nonuniform broadening of the XRD peaks observed in the hematite products.

INTRODUCTION

Geothite (α-FeOOH) is transformed into hematite (α-Fe_2O_3) through a dehydration process accompanied by the structural change from orthorhombic to rhombohedral. This transformation has been extensively studied by various methods such as X-ray and electron diffractions (1–4), IR spectroscopy (5), and adsorption of various gases (6–8). It has been concluded that hematite is formed in a closed orientation relationship with the original goethite. The *a*, *b*, and *c* axes of the goethite cell become through the topotactic reaction the *c*, *a*, and $(1\bar{1}0)$ directions of the hematite cell, respectively (2, 4). The powder IR spectra of hematite products can vary depending on the temperature at which they are formed, and can be interpreted to effects of particle size and shape (5). Finally, the surface area of microcrystals increases remarkably in the dehydration process of α-FeOOH due to the micropore formation during the goethite decomposition (7, 8). However, minor attention has been paid to the complete pore structure evolution during the reaction.

In the present work, a detailed study of the thermal treatment *in air* of synthetic goethite has been carried out up to 1000°C by means of X-ray powder diffraction (XRD), transmission electron microscopy (TEM), IR spectroscopy, and nitrogen adsorption.

EXPERIMENTAL

Materials

Synthetic goethite was obtained following the procedure of Atkinson *et al.* (9). Electron micrographs showed acicular morphology for the particles, with an average size of about 0.4×0.08 μm. The thermal decomposed samples were obtained by heating for 2 hr the original goethite ($\sim$1 g) in air at several temperatures up to 1000°C. The sample nomenclature employed indicates the temperature of treatment.

[1] Present address: Departamento de Química Inorgánica, Facultad de Ciencias, Universidad de Córdoba, Spain.

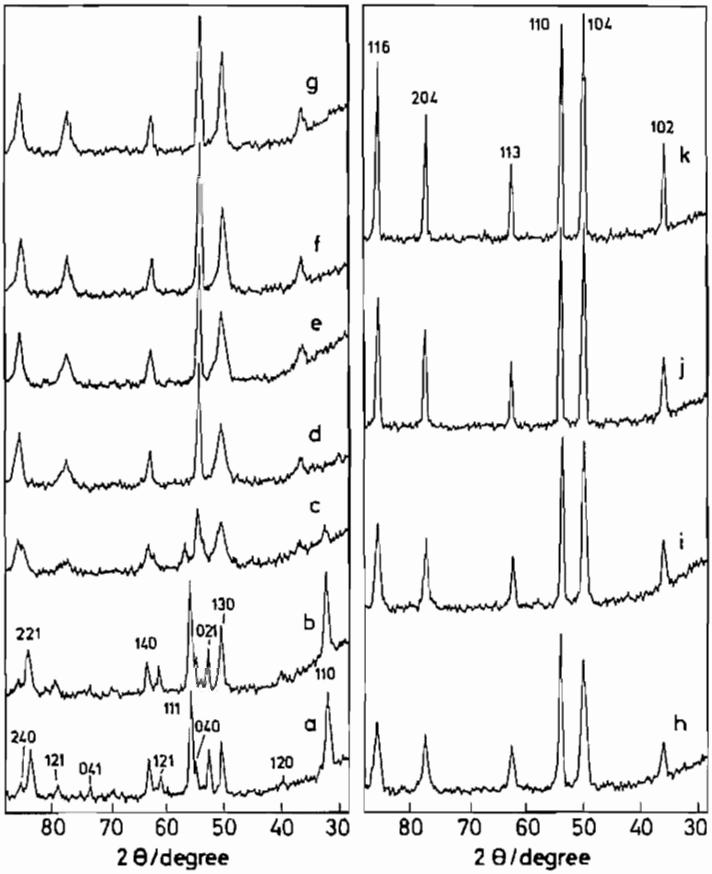

FIG. 1. XRD powder patterns of samples obtained by heating α-FeOOH *in air* for 2 hr at: (a) 25°C (original sample); (b) 150°C; (c) 200°C; (d) 250°C; (e) 300°C; (f) 350°C; (g) 400°C; (h) 500°C; (i) 600°C; (j) 800°C; and (k) 1000°C.

Apparatus and Procedures

XRD patterns of samples were measured by a Philips PW-1010 diffractometer with Cr$K\alpha$ radiation. IR absorption spectra were recorded using KBr pellets on a Perkin–Elmer 580 B spectrophotometer and electron micrographs were taken from a Siemens Elmiskop 102 apparatus.

The adsorption of nitrogen gas (99.9% purity) was measured at 77°K in a conventional volumetric apparatus. The samples were previously equilibrated in a vacuum better than 10^{-4} mm Hg for at least 2 hr at room temperature. Surface areas were calculated using the BET (10) and *t*-plot (11) procedures, the latter was used as a method of assessing microporosity. Mesopore analysis was carried out using the Dollimore and Heal method (12), assuming cylindrical geometry for the pores for the reason given below.

RESULTS

X-Ray Diffraction

XRD patterns of undecomposed and decomposed samples are shown in Fig. 1. The peaks of sample GT/25 (original goethite) and GT/150 coincide with those of α-FeOOH (13), and no impurities were detected in the GT/25 sample. The sample GT/200 was a mixture of both products goethite and hematite and the decomposition was almost

complete at 250°C, eliminating the α-FeOOH peaks in the corresponding diagram. A nonuniform broadening of the XRD peaks is observed for the sample GT/250 and the broad peaks change into sharp ones on heating above 600°C (Fig. 1). As can be seen, the crystallinity of hematite products improves with the temperature of formation.

Infrared Analysis

Hematite (D_{3d}^6 symmetry) gives six infrared active vibrations, two A_{2u} ($E \| C$) and four E_u ($E \perp C$), consistent with the IR reflection spectrum of α-Fe_2O_3 measured by Onari *et al.* (14) in the 30–1000 cm^{-1} range (Table I).

IR spectra of decomposed samples in the 200–800 cm^{-1} range are shown in Fig. 2. No absorption bands of α-FeOOH are observed in the IR spectrum of sample GT/250, in agreement with XRD observations. It can be noticed that a rather invariable IR spectrum is obtained in the 250–600°C temperature range, whose main absorption bands are listed in Table I. However, significant differences are observed in the IR spectra corresponding to hematites formed above 600°C.

TABLE I

Infrared Lattice Vibrations of α-Fe_2O_3

Assignment		Crystal[a]	Powder (lath-shaped)
A_{2u}	ω_L	662	650
	ω_T	526	
E_u	ω_L	662	525
	ω_T	524	
E_u	ω_L	494	440
	ω_T	437	
A_{2u}	ω_L	414	400
	ω_T	299	
E_u	ω_L	386	300
	ω_T	286	
E_u	ω_L	230	230[b]
	ω_T	227	

[a] Onari *et al.*, 1977.
[b] Observed on CsI crystal.

Nitrogen Adsorption

Adsorption isotherms of N_2 at 77°K are shown in Fig. 3. They are of type II in the BDDT classification (15) and, excluding those corresponding to samples obtained above 600°C, they exhibit hysteresis which in each case extends down to low relative pressure, $P/P_\circ$.

t-Plots are given in Fig. 4. In the construction of these plots the values of t (statistical thickness of the N_2 adsorbed layer on the nonporous reference surface) have been obtained from the standard isotherms reported by Lecloux and Pirard (16) for different values of the C parameter of the BET equation. Two straight lines are obtained for samples GT/200 and GT/250, the intersection located at about 0.6 nm for both samples. This indicates the presence of micropores of nearly equal size in both samples. Upward deviations in the corresponding *t*-plots are observed for samples obtained up to 600°C, indicating enhanced adsorption due to capillary condensation of N_2 in mesopores. On the other hand, one straight line passing through the origin is obtained for samples formed above 600°C, showing absence of porosity.

Surface areas obtained by the BET, S_{BET}, and *t*-plot, S_t, methods (Table II) are in close agreement, indicating the correctness in the choice of the standard isotherms employed in the *t*-plots and, consequently, both methods give a reliable surface area for the present hematite samples.

Cumulative surface areas, S_{cum}, and cumulative volumes, V_{cum}, in the mesopore range are included in Table II. The same t values as used in the corresponding *t*-plots are employed in the analysis. A good agreement is observed between S_{BET} and V_p values (the latter have been directly read from the isotherms at $P/P_\circ = 0.95$), except for samples GT/200 and GT/250 for which the agreement is worst, because the micropores

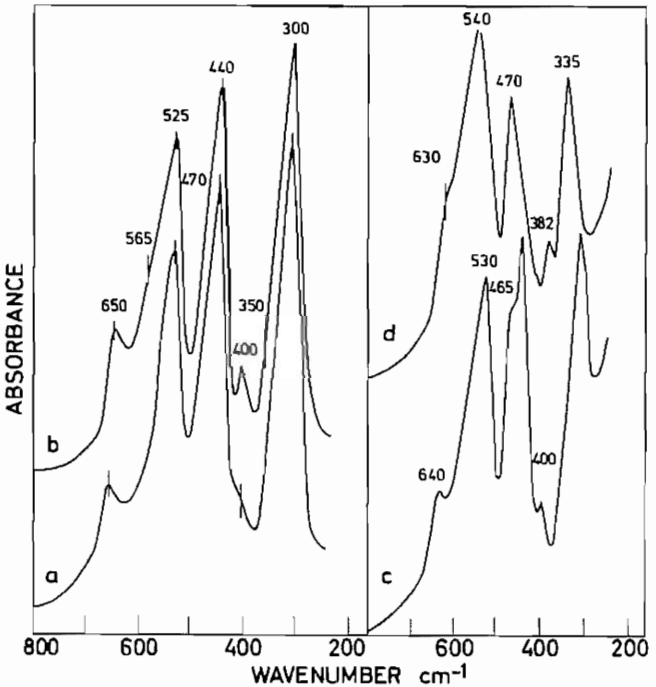

FIG. 2. IR spectra of hematite products obtained in the range 250–950°C: (a) GT/250; (b) GT/600; (c) GT/700; and (d) GT/950. All samples were pressed in KBr pellets.

are not taken into account in the present mesopore analysis. For such microporous adsorbents, both the total area, S_t, and the external area, S_{ex}, are calculated from the slopes of the initial steep line and the less steep line after intersection in the *t*-plot, respectively. On the other hand, the micropore volume, V_{mp}, is estimated by extrapolating the less steep line above intersection to the ordinate (17). These values are summarized in Table III. The difference between S_{BET} and S_{ex} may be assumed as micropore surface area, S_{mp}. The sums $S_T = S_{cum} + S_{mp}$ and $V_T = V_{cum} + V_{mp}$ (Table III) agree rather well with the corresponding S_{BET} and V_p values for both samples GT/200 and GT/250.

Electron Microscopy

Treated samples were examined by TEM, and the corresponding micrographs are shown in Fig. 5. It can be clearly observed in sample GT/250 (Fig. 5a) a number of slit-shaped micropores running parallel to the elongated direction of the acicular hematite microcrystals, the (1$\bar{1}$0) hematite direction (2, 4). Their average width was determined to be about 1.4 nm. The crystal size between two slits was determined to be less than 3 nm. This microporosity is destroyed at higher temperatures of treatment, a nearly spherical mesopore structure appearing, which is clearly visible at 500°C (Fig. 5b). Above 600°C, interparticle sintering takes place (Fig. 5c) and no pore structure is observed.

DISCUSSION

Three stages may be differentiated during the dehydration process of α-FeOOH: (i) 200–250°C, (ii) 300–600°C, and (iii) above 600°C, which will be discussed separately.

200–250°C. At this stage, mixtures of both materials goethite and hematite are obtained until the temperature reaches 250°C at which the reaction is almost complete, as can be

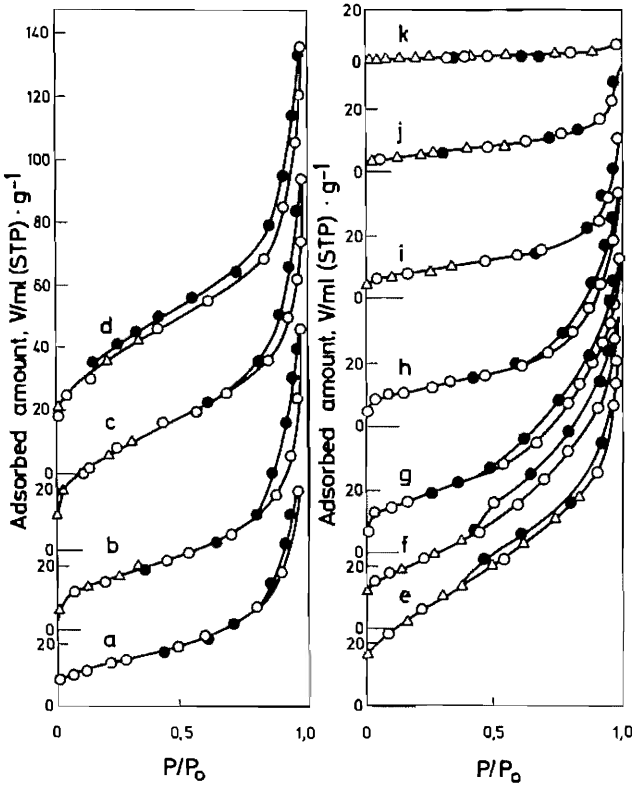

FIG. 3. N_2 adsorption isotherms at 77°K on original and decomposed samples. The same symbology as in Fig. 1 is used (△, ○, ads.; ●, des.).

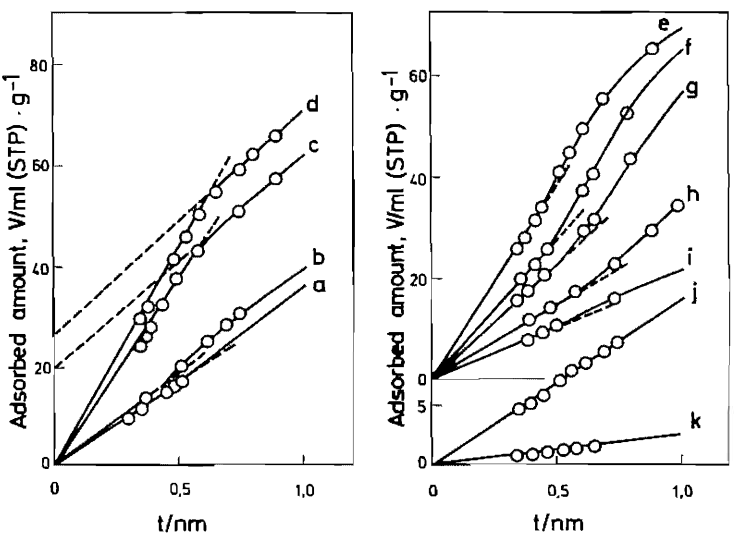

FIG. 4. *t*-Plots of original and decomposed samples. See Figs. 1 and 3.

TABLE II

Results from N_2 Adsorption at 77°K

T (°C)	C	$m^2\ g^{-1}$				ml g^{-1}		
		S_{BET}	S_t	S_{cum}	%[a]	V_p	V_{cum}	%[b]
25	90	49.7	51.1	42.2	15.1	0.1090	0.1035	5.1
150	130	57.7	57.5	53.0	8.2	0.1504	0.1461	2.9
200	105	111.3	116.3	78.8	29.2	0.1869	0.1680	10.1
250	105	131.8	133.9	87.7	33.4	0.2126	0.1845	13.2
300	45	114.6	115.3	100.3	13.6	0.1757	0.1648	6.2
350	60	82.6	83.5	95.6	−15.7	0.1581	0.1592	−0.7
400	70	66.7	68.4	72.5	−8.7	0.1497	0.1489	0.5
500	275	42.6	44.6	39.2	8.0	0.1183	0.1147	3.0
600	110	31.5	31.3	25.7	18.4	0.0812	0.0776	4.4
800	60	19.7	20.5	16.3	17.3	0.0434	0.0410	5.5
1000	50	3.2	3.3	—	—	0.0080	—	—

[a] $[(S_{BET} - S_{cum})/S_{BET}] \times 100$.
[b] $[(V_p - V_{cum})/V_p] \times 100$.

demonstrated by XRD (Fig. 1) and IR (Fig. 2) observations. External appearances of the decomposed samples (Fig. 5a) resemble those of the original goethite, i.e., the decomposition reaction occurs within a microcrystal without significant changes in crystal size and shape.

The N_2 adsorption isotherm corresponding to sample GT/250 shows low pressure retention (Fig. 3d). This kind of retention has been previously found in the N_2 adsorption by some aluminum oxyhydroxides (18), chromium oxide gels (19), and orthorhombic CrOOH (20). TEM observations show the presence of slit-shaped micropores in the hematite microcrystals (Fig. 5a). This microporosity is corroborated by downward deviations in the corresponding t-plots (Figs. 4c and d). For such micropores, the width, d_s, is expressed by $d_s = 2(V_{mp}/S_{mp})$, where V_{mp} and S_{mp} refer to the micropore volume and area, respectively (Table III). The calculated values of d_s are 1.32 and 1.28 nm for GT/200 and GT/250, respectively, in close agreement with twice the t value of 0.6 nm obtained from the intersection of the two straight lines observed in t-plots (Figs. 4c and d), and with the average slit width of about 1.4 nm observed by TEM (Fig. 5a). It should be mentioned that this slit-shaped microporosity has been also observed in the thermal decomposition of α-FeOOH *in vacuo* at 300°C for 4 hr (8). In contrast, in the case of orthorhombic CrOOH, this slit-shaped microporosity has been reported to occur during its decomposition above 350°C for 15

TABLE III

Complete Pore Analysis of Microporous Samples GT/200 and GT/250

T (°C)	$m^2\ g^{-1}$					ml g^{-1}			
	S_{BET}	S_{ex}	S_{mp}	S_T	%[a]	V_p	V_{mp}	V_T	%[b]
200	111.3	61.6	49.7	128.5	15.5	0.1869	0.0328	0.2008	7.4
250	131.8	66.9	64.9	152.7	15.9	0.2126	0.0416	0.2261	6.4

[a] $[(S_T - S_{BET})/S_{BET}] \times 100$.
[b] $[(V_T - V_p)/V_p] \times 100$.

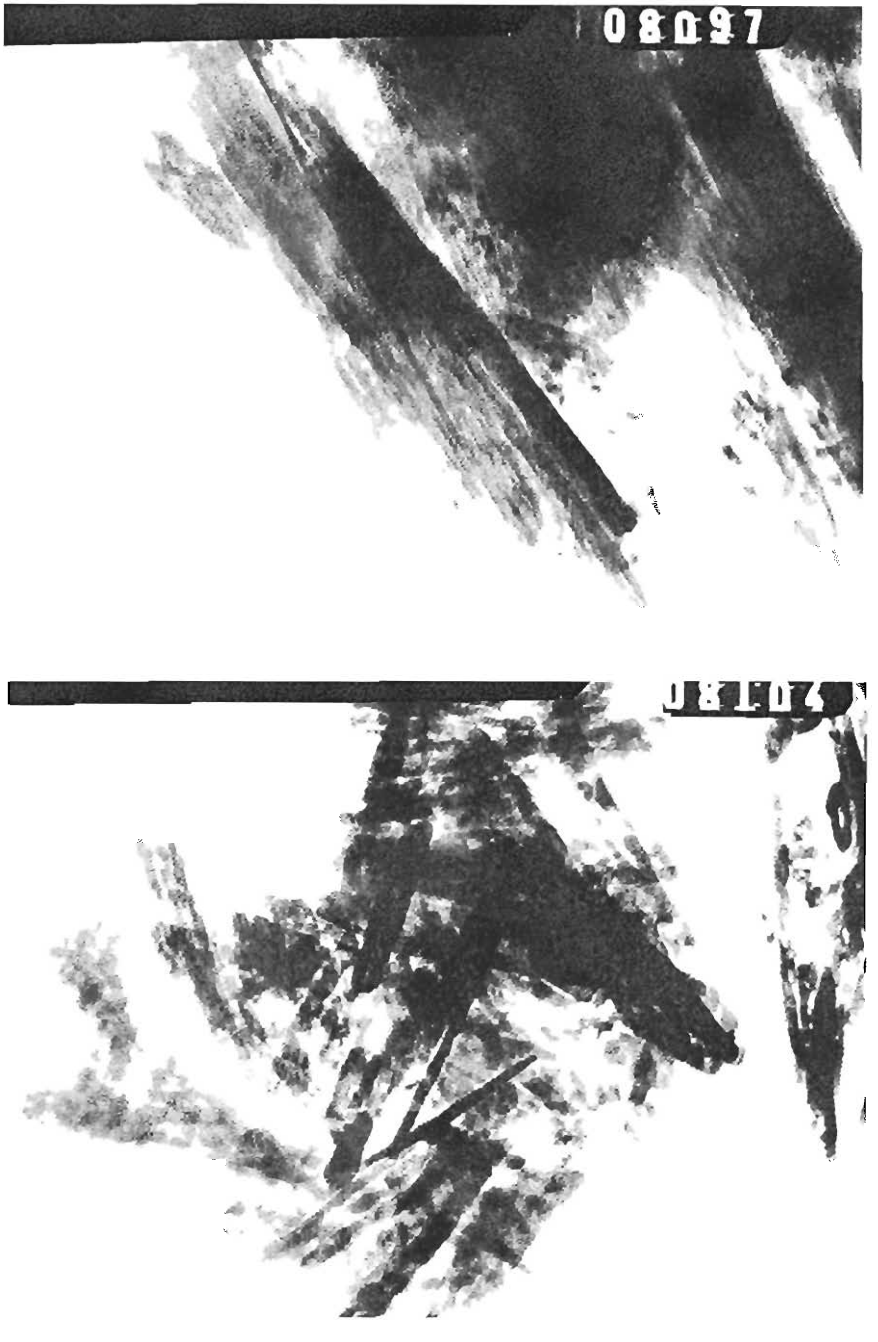

FIG. 5. Electron micrographs of samples (a) GT/250 (×200,000); (b) GT/500 (×50,000); and (c) GT/950 (×30,000).

min *in vacuo* (20), but no microporosity was observed when the thermal decomposition is carried out *in air* (21).

The IR absorption bands of GT/250 are listed in Table I. From the work of Ruppin and Englman (22) it became clear that par-

FIG. 5—*Continued.*

ticle size and shape have a great influence in the IR spectrum of a polar crystal. For a particle size much smaller than the radiation wavelength, which is the case of this hematite, only absorptions due to surface modes should appear in the IR spectrum, lying between their crystal transverse (ω_T) and longitudinal (ω_L) absorptions (22). Thus, the IR absorption bands of powder GT/250 have to be interpreted in terms of particle shape. Classical scattering theory (23, 24) applied to lath-shaped α-Fe_2O_3 particles predicts the IR absorptions observed in Fig. 2a (25). According to that, the bands at 650 and 400 cm^{-1} have transition moments parallel to the c axis (A_{2u}) whereas those at 525, 440, and 300 cm^{-1} have transition moments perpendicular to c (E_u). On the other hand, experimental evidence for this assignment has been shown (5). It can be seen in Table I that the A_{2u} and E_u powder absorptions are close to ω_L and ω_T, respectively. Therefore, these "surface modes" are unaffected by the medium dielectric constant (5). These features suggest that the acicular crystals observed in TEM for GT/250 have really a lath-like morphology with their thickness much smaller than the other two dimensions.

300–600°C. Since particle size and shape are unaffected during this stage (Fig. 5b), an invariant IR spectrum is obtained for hematites formed throughout this temperature range (Fig. 2b). The micropores have been destroyed and these pores transform into closed spherical mesopores (Fig. 5b), due to an internal sintering which brings about more crystal homogeneity (4). *t*-Plots corroborate the absence of microporosity (Fig. 4) and the analysis of mesopores gives cumulative values in close agreement with those total ones (Table II). The assumption of cylindrical pore geometry, as claimed by the method employed (12), clearly applies in this case of nearly spherical pores (Fig. 5b).

Above 600°C. Interparticle sintering occurs within this stage of reaction, leading to a heterogeneity in particle size and shape (Fig. 5c). Subsequently, the IR spectra of he-

matite products differ markedly depending on heating temperature, i.e., the rate of sintering (Figs. 3c and d). Ionic powders show usually broad absorption bands, presumably due to large anharmonicity contribution (26) or to particle aggregation (27). Nevertheless, when these effects are taken into account, the experimental IR spectra of Figs. 3c and d can be reproduced for combination of particles with different geometries (25, 28). At this stage, the internal sintering is complete and, therefore, no appreciable pore structure is observed neither by TEM observations (Fig. 5c) nor by *t*-plots (Fig. 4). The N_2 adsorption isotherms are completely reversible (Fig. 3).

In connection with above textural considerations, it may be important to examine the nonuniform broadening of the XRD peaks observed in GT/250 (Fig. 1). The (102), (104), and (204) peaks are very broad, whereas the (110), (113), and (116) ones are sharper. As this effect decreases on further heating, some authors (1, 2) believe that this nonuniform broadening is correlated to some crystal imperfections, strains, or faults occurring at low temperature of decomposition. Naono and Fujiwara (8) correlated the nonuniform broadening to the presence of slit-shaped micropores in acicular hematite crystals. However, Duvigneaud and Derie (4) have recently shown that the nonuniform broadening is due to shape anisotropy of the particles rather than to strain and fault broadenings since (i) the phenomenon was negligible in spherical-shaped particles; (ii) the nonuniform broadening remains in acicular particles after further heating at 600°C; and (iii) a good estimate of the ratio of the particle width and thickness was found. They concluded that, as in our case, the hematite acicular particles were lath-shaped. In agreement with (4), the nonuniform broadening remains even at 600°C prior to the sintering process which affects the particle lath morphology (Fig. 1).

ACKNOWLEDGMENTS

Thanks are due to Mr. L. Puebla and Mrs. M. A. Muro for technical assistance.

REFERENCES

1. Rooksby, H. P., *in* "X-Ray Identification and Structures of Clay Minerals," p. 376. Mineralogical Society, London, 1961.
2. van Oosterhout, G. W., *Acta Crystallogr.* **13,** 932 (1960).
3. Lima-de-Faria, J., *Z. Kristallogr.* **119,** 176 (1963).
4. Duvigneaud, P. H., and Derie, R., *J. Solid State Chem.* **34,** 323 (1980).
5. Rendón, J. L., and Serna, C. J., *Clay Miner.* **16,** 375 (1981).
6. Jurinak, J. J., *J. Colloid Sci.* **19,** 477 (1964).
7. Bye, G. C., and Howard, C. R., *J. Appl. Chem. Biotechnol.* **21,** 324 (1971).
8. Naono, H., and Fujiwara, R., *J. Colloid Interface Sci.* **73,** 406 (1980).
9. Atkinson, R. J., Posner, A. M., and Quirk, J. P., *J. Phys. Chem.* **71,** 550 (1967).
10. Brunauer, S., Emmett, P. H., and Teller, E., *J. Amer. Chem. Soc.* **60,** 309 (1938).
11. Lippens, B. C., and de Boer, J. H., *J. Catal.* **4,** 319 (1965).
12. Dollimore, D., and Heal, G. R., *J. Colloid Interface Sci.* **33,** 508 (1970).
13. Smith, J. V., Ed., Index to the X-Ray Powder Data File, ASTM (1962), File No. 17-536 and 13-534.
14. Onari, S., Arai, T., and Kudo, K., *Phys. Rev. B* **16,** 1717 (1977).
15. Brunauer, S., Deming, L. S., Deming, W. E., and Teller, E., *J. Amer. Chem. Soc.* **62,** 1723 (1940).
16. Lecloux, A., and Pirard, J. P., *J. Colloid Interface Sci.* **70,** 265 (1979).
17. Sing, K. S. W., *Chem. Ind.* 829 (1967).
18. Aldcroft, D., Bye, G. C., Robinson, J. G., and Sing, K. S. W., *J. Appl. Chem.* **18,** 301 (1968).
19. Baker, F. S., Carruthers, J. D., Day, R. E., Sing, K. S. W., and Stryker, L. J., *Discuss. Faraday Soc.* **52,** 173 (1972).
20. Alario-Franco, M. A., and Sing, K. S. W., *Anal. Quim.* **71,** 296 (1975).
21. Saez-Puche, R., Alario-Franco, M. A., and Torralvo, M. J., *in* "Characterization of Porous Solids" (S. J. Gregg, K. S. W. Sing, and H. F. Stoeckly, Eds.), p. 127. SCI, London, 1979.
22. Ruppin, R., and Englman, R., *Rep. Progr. Phys.* **33,** 149 (1970).
23. van de Hulst, H. C., "Light Scattering by Small Particles," p. 63. Wiley, New York, 1957.
24. Iglesias, J. E., Rendón, J. L., and Serna, C. J., *Appl. Spectrosc.* **36,** 325 (1982).
25. Serna, C. J., Rendón, J. L., and Iglesias, J. E., *Spectrochim. Acta* **38A,** 797 (1982).
26. Genzel, L., and Martin, T. P., *Phys. Status Solidi (B)* **51,** 91 (1972).
27. Clippe, P., Evrard, E., and Lucas, A. A., *Phys. Rev. B* **14,** 1715 (1976).
28. Rendón, J. L., Iglesias, J. E., and Serna, C. J., *Opt. Pura Appl.* **14,** 117 (1981).